The Report committee for John Grant MacKay
Certifies that this is the approved version of the following report:

Efficient Magnet Configuration for Low-Field Nuclear Magnetic Resonance Applications

SUPERVISING COMMITTEE:

Jacob Abraham, Supervisor

Ranjit Gharpurey

Efficient Magnet Configuration for Low-Field Nuclear Magnetic Resonance Applications

by

John Grant MacKay

Report

Presented to the Faculty of the Graduate School
of the University of Texas at Austin
in Partial Fulfillment
of the Requirements
for the Degree of

Master of Science in Engineering

The University of Texas at Austin
May 2019

Acknowledgments

I would like to thank all those who have supported me to reach this achievement. To those who have lifted me up and encouraged me, I sincerely thank you.

Special thanks to Dr. Jacob Abraham and Dr. Ranjit Gharpurey for guiding me during this work. Thank you to Dr. Brian Evans for helping me transition to UT Austin, and to Dr. Yale Patt for showing me how much I can achieve. To all my friends, thank you for providing me the balance and fun in my life. To Jaclyn, your love and support has helped me more than you know. And to my family, for all the sacrifices you have made to help me achieve, and for your unending support.

Efficient Magnet Configuration for Low-Field Nuclear Magnetic Resonance Applications

by

John Grant MacKay, M.S.E.
The University of Texas at Austin, 2019
SUPERVISOR: Jacob Abraham

By miniaturizing instrumentation, nuclear magnetic resonance (NMR) can be brought into new domains and potentially revolutionize molecular analysis. The key towards miniaturization is using a small, portable magnet while maintaining strict field homogeneity. This work presents novel annulus designs as well as implementations of the previously researched Halbach array. The annulus designs, although competitive in field strength, lack the required homogeneity for NMR applications. However, experimental results show the Halbach array has the best homogeneity of our magnet configurations and can readily be adopted for NMR relaxometry. With modest additions, the Halbach array may also be a viable magnet design for NMR spectroscopy. Impressive homogeneity results combined with low-cost (under $3.00), portability, and ease of construction show the presented magnet design can make a significant impact in miniaturizing NMR devices and expanding NMR applications.

Table of Contents

List of Tables

List of Figures

Chapter 1

Introduction

Nuclear Magnetic Resonance (NMR) is a physical phenomenon observed in almost all atomic nuclei. The basic principle is that nuclei with non-zero spin will absorb, and consequently emit, photons of a certain resonant frequency when aligned to an external magnetic field. Because the resonant frequency differs for certain nuclei, NMR can be used to identify the properties of an unknown sample. This is the basic premise of NMR spectroscopy, where the principles of NMR are used to identify molecules. Magnetic resonance is also used in technologies such as MRI (magnetic resonance imaging) which employs multi-dimensional NMR measurements [6, 18, 22, 23].

NMR spectroscopy instrumentation has recently been trending towards smaller, more portable magnets. This is motivated primarily by the costs associated with existing superconducting NMR spectrometers; superconducting magnets require very expensive cooling systems and take up entire laboratories. This cost prevents many from conducting NMR-based research.

However, even with newer commercially available "bench-top" NMR spectrometers, cost is a limitation. Table 1.1 below provides information about the top four commercial NMR spectrometers available in late 2018. All these

Name	**Year**	**Freq (MHz)**	**Resolution (Hz)**	**Field Strength (T)**	**Weight (lbs)**	**Price**
Spinsolve	2017	80 60 42.5	<0.5	1.9 1.4 1.0	161 132 121	$40,000- $120,000
picoSpin	2009 2013	45 82	<1.8 1.48	1.0, 2.0	10, 41	N/A
NMReady	2015	60	1.2	1.4	55	$39,525- $59,525
Pulsar	2013	60		1.4	375	$85,000

Table 1.1: Information regarding commercial "bench-top" NMR spectrometers available in 2018. All information from companies' websites.

systems forgo the superconducting magnets for smaller, cheaper, permanent rare-earth magnets. The frequencies listed for the spectrometers refers to the Larmor frequency of the ^{1}H nucleus.

The available commercial spectrometers use permanent magnets in the 1.0-2.0 T range, which corresponds to a resolution of roughly 1 Hz. This means that the spectrometers are able to distinguish peaks up to 1Hz apart, but anything closer together will be overlapping in the Fourier Transform. As seen in Section 2.3.2, increased resolution (smaller frequency) is necessary to view the chemical shifts of compounds. This resolution is essential for those examining complex compounds, but perhaps is not necessary for all users. For example, NMR relaxometry measures the time-domain NMR signal and can tolerate much lower resolutions.

The largest limitation to these commercial products is obviously the price. However, another serious concern is the portability. Despite shrink-

ing NMR instrumentation from the size of a room, benchtop NMR's limited portability prevents widespread and versatile usage. For example, NMR spectroscopy is currently limited to chemical analysis of compounds, with some analysis of food for nutritional information. But, to what other domains could we apply NMR technology if it were no longer tethered to a laboratory?

One of our interests is bringing NMR instrumentation into the medical profession for quick diagnostics. Imagine if your doctor could use a handheld, portable NMR device to analyze a blood sample or tissue. Just as we use NMR to analyze chemical compounds in chemistry labs, what if we could gather data necessary for quicker medical diagnostics?

Our motivation follows from this use case. We aim to create a low-field magnet for NMR applications that is smaller, more portable, and cheaper than the existing magnets used in NMR devices. We hope future work can take advantage of our magnet design to create miniaturized NMR instrumentation, which can then be used in a plethora of new applications such as medical diagnostics.

This report is structured as follows. Chapter 2 describes the basics of nuclear magnetic resonance and how NMR instrumentation is designed. Chapter 3 discusses how the magnets used in NMR instrumentation are designed. Chapter 4 discusses the experimental setup of this work. Chapter 5 presents data obtained from our experiments, and Chapter 6 gives analysis and directions of future work. Chapter 7 concludes the report, with appendices found at the end of this document.

Chapter 2

Nuclear Magnetic Resonance

2.1 Background

From quantum mechanics, it is known that electrons have quantized levels of spin, usually thought of as "up spin" (+1/2) and "down spin" (-1/2) [12]. Similarly, atomic nuclei also exhibit quantized spin-levels. But unlike electrons, atomic nuclei can have zero spin, which is usually found in atoms with an even number of protons and neutrons [2]. In these nuclei, such as ^{12}C, ^{16}O, and ^{32}S, there is no atomic magnetic moment and therefore NMR is not observed. However, in all other atomic nuclei with a non-zero spin, a magnetic moment occurs. This magnetic moment can be thought of qualitatively as the result of a spinning charged particle.

$$\boldsymbol{\mu} = \gamma \times \boldsymbol{p} \tag{2.1}$$

$$p = I \times \hbar = \frac{I \times h}{2\pi} \tag{2.2}$$

where $\boldsymbol{\mu}$ is the magnetic moment vector, γ is the gyromagnetic ratio (which is different for all nuclei), $\boldsymbol{p}$ is the angular momentum vector, I is the atomic spin number, and h is Planck's constant.

2.2 Magnetic Resonance

When an atomic nucleus with a non-zero spin is put into an external magnetic field, the nucleus' magnetic moment will attempt to align to the external magnetic field. Using a classical mechanics analogy, this can be thought of as the external magnetic field applying a torque to the nucleus' magnetic moment. This torque causes the nucleus to precess similar to a spinning top, as shown in Figure 2.1 below.

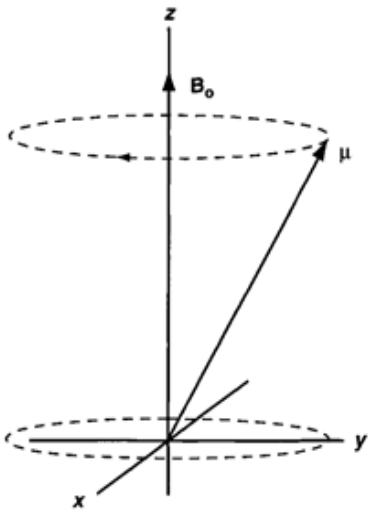

Figure 2.1: Classical representation of Larmor precession. Adapted from *High Resolution NMR* by Becker [2].

The frequency at which the magnetic moment rotates is the resonant frequency of the nucleus, which is called the Larmor frequency in the context of NMR. The Larmor frequency is linearly related to the strength of the external

magnetic field through the following equations [23]:

$$\begin{gathered}\omega \ = \gamma \times B \\ (Angular\ frequency,\ rad/s)\end{gathered} \tag{2.3}$$

$$\begin{gathered}v = \gamma \times \tfrac{B}{2\pi} \\ (Frequency,\ Hz)\end{gathered} \tag{2.4}$$

Where γ is the gyromagnetic ratio and B is the magnetic field strength in Teslas. Although the nuclear spin numbers are fixed to relatively few values, the variation in the gyromagnetic ratio allows for a wide spectrum of Larmor frequencies for different nuclei. This variation provides the foundation for NMR measurement techniques, which are discussed later.

Though the precession analogy clarifies the interaction of the external magnetic field and magnetic moment, a quantum mechanical explanation provides more insight into the nature of magnetic resonance; instead of using vectors and torques, energy-states provide a clearer understanding. When exposed to the external magnetic field, the nucleus aligns itself with the field. There are two energy states possible for the nucleus within the field: a low-energy state and a high-energy state. Most nuclei will naturally align to the low-energy state. The difference between the two energy states is derived through quantum mechanics and arrives at a convenient conclusion [2].

$$E = h \times v = h \times \gamma \times \frac{B}{2\pi} \tag{2.5}$$

The energy difference is directly proportional to the Larmor frequency and therefore the strength of the external magnetic field. If a photon with

matching energy interacts with the nucleus, it will absorb the photon and transition to the higher energy state [6, 22, 23]. This is done by exposing the nuclei to RF radiation at the Larmor frequency. Once the RF radiation is removed, the nucleus will transition back to the lower energy state. During this transition, it will emit a photon with energy corresponding to the energy difference between the two states. Therefore, once the RF radiation is removed, the nuclei will emit RF radiation of its own at the same Larmor frequency [6, 22]. This emitted RF signal is what is recorded in NMR experiments.

In summary, NMR physics works as follows. An atomic nucleus with a magnetic moment (non-zero spin) is aligned in an external magnetic field. When exposed to a pulse of RF radiation at the Larmor frequency, the nucleus will emit a matching RF signal.

2.3 NMR Spectroscopy

2.3.1 Theory

Because the nuclei of different atoms have different gyromagnetic ratios, the Larmor frequencies of various nuclei vary. Researchers realized the unique Larmor frequencies could be used to identify an unknown substance, which is the basis of NMR spectroscopy. In NMR spectroscopy, an unknown sample is placed in a strong external magnetic field. When the sample absorbs and then emits photons, the RF signal is captured and measured. From this signal, the Larmor frequency of the sample can be determined which gives insight to the chemical makeup of the sample.

In general, there are five components to NMR spectrometers. The first is a magnet, which will be discussed in Chapter 3. This is used to align the sample's magnetic moments. The second component is an RF transmitter which generates the external RF signal. Third is an RF coil which is used to measure the response from the sample. Fourth is the electronics necessary to analyze the generated RF signal. Finally, the sample to be measured.

There are two standard ways of generating the RF signal from the sample. The first is the simpler "continuous wave" (CW) experiment in which the external RF signal frequency is kept constant, but the magnetic field strength varies. Once the magnetic field causes the sample to precess at the Larmor frequency, the external RF signal will excite the atomic nuclei to the higher energy state, which will then generate a RF response as the stimulus is removed. The magnetic field sweeps to find the Larmor frequency.

The second way is by varying the RF signal. The sample is placed in a strong external magnetic field which is kept constant. RF radiation is then pulsed at the sample, sweeping its frequency. When the radiation matches the Larmor frequency, an RF response will be generated. This is known as Fourier-Transform (FT) NMR because the RF response is measured in time as it decays. A Fourier transform is used to extract the frequency pattern from the signal.

2.3.2 Chemical Shift

It has been discussed how NMR spectroscopy can be used to analyze an atomic nucleus to find its identity. However, it is rarely necessary to identify the properties of a sample with a single chemical element. What is more useful is using NMR spectroscopy to identify chemical compounds and molecules. By analyzing various Larmor frequencies, NMR spectroscopy observes multiple frequency peaks which correspond to different atomic nuclei. This information can then be used to identify the various atoms that make up a specific sample. However, there are two limitations to this: first, atoms with zero nuclear spin cannot be observed, and second the peaks do not indicate the actual configuration of a molecule. More information is required to identify specific chemical molecules instead of their atomic components.

Just as atomic nuclei produce a magnetic moment due to their spin, electrons surrounding atomic nuclei also have a magnetic moment. The electrons can be thought of as either shielding or deshielding the nucleus from the magnetic field, thus affecting the observed Larmor frequency. This interaction is observed in NMR signals by an apparent shift of the resonant frequency, known as the chemical shift [21]. The exact amount of resonant frequency shifting is unique to different molecules. Therefore, just as the distinct Larmor frequency is used to identify nuclei, the chemical shift gives insight to the structure and identity of the compound being sampled. In this way, NMR spectroscopy can be used to identify a wide variety of chemical compounds with great accuracy.

2.3.3 Homogeneity

A key requirement of NMR spectroscopy is having a homogeneous external magnetic field applied to the sample [2]. With a homogeneous field, all nuclei in the sample are affected similarly and exhibit the same Larmor frequency. When the RF signal is recorded and analyzed, this results in a clean peak at the Larmor frequency and high signal resolution. This also allows for high sensitivity to chemical shifts, as small frequency changes appear as distinct peaks. Additionally, if there are multiple molecules with peaks at similar frequencies, the homogeneous field will cause those peaks to not overlap.

If the field is inhomogeneous, different nuclei will observe slightly different external magnetic fields, resulting in different Larmor frequencies. When a Fourier transform is applied to this signal, the overlapping peaks will result in a wider frequency response. Information regarding multiple Larmor peaks and chemical shifts may then be lost. A visual example of homogeneity changes resulting in greater resolution is seen below in Figure 2.2.

Historically, NMR spectrometers employed extremely large field superconducting magnets to ensure the field was homogeneous. These superconducting magnets can have field strength of 23 T [26], which by comparison is almost an order of magnitude stronger than the magnetic field used in MRI machines. Other techniques used to increase magnetic field homogeneity include using shim coils, which modify the magnetic field with adjustable currents, and spinning the sample to average out any inhomogeneity [2].

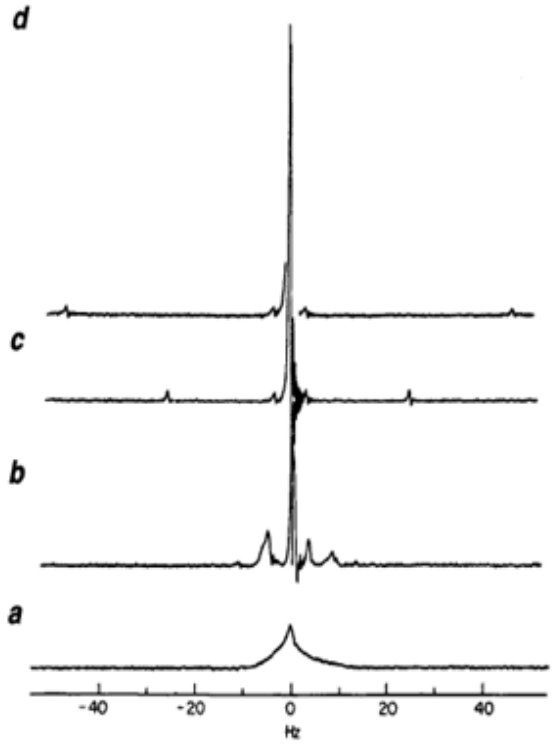

Figure 2.2: Examples of increasing homogeneity. (a) Has no sample spinning, (b) spun at 4 rev/s, (c) spun at 25 rev/s, and (d) spun at 46.5 rev/s. As homogeneity increases, resolution/sensitivity improves and frequency line width decreases. Adapted from *High Resolution NMR* by Becker [2].

Typically, magnetic field homogeneity is measured in ppm (parts per million), where a single ppm is one one-millionth of the magnetic field strength. For NMR spectroscopy of the ^1H nucleus, detection of carbon-based compound chemical shifts requires a field homogeneity of 12ppm over the measured volume, which is roughly $1cm^3$ [2]. However, larger and more complex compounds can tolerate larger inhomogeneity on the order of 100ppm [7].

2.4 NMR Relaxometry

An alternative application of nuclear magnetic resonance is known as NMR relaxometry. Instead of analyzing frequency-domain signals, relaxometers analyze the NMR time-domain signal. Once the RF signal used to excite the nucleus is removed, the nucleus will "relax" into its lower energy spin-state [2]. There are two components of this relaxation, which can be observed qualitatively in the frequency-domain signal. The first component is a loss of signal intensity, known as the T_1 process. The second component is associated with a widening of the signal, known as the T_2 process.

More specifically, the T_1 process occurs when multiple nuclei in a sample relax to their original spin-states, aligned in the external magnetic field. After a time period of T_1, which can last milliseconds to seconds, the sample settles at its pre-RF signal equilibrium. This is known as the spin-lattice relaxation time, which observes an exponential decay as seen in equation 2.6.

$$M_z(t) = B_0(1 - e^{-t/T_1}) \tag{2.6}$$

The T_2 process is due to the spin interactions of different nuclei. Due to random variations in the magnetic field, nuclei precess at slightly different Larmor frequencies. This leads to some of the nuclei being out of phase with each other in their magnetic moments. As the RF signal is removed and the nuclei relax into equilibrium, these dephased nuclei interact with each other and produce another exponential decay signal. This is known as the spin-spin

relaxation time, which is shown in equation 2.7.

$$M_{xy}(t) = M_{xy}(0)e^{-t/T_2} \tag{2.7}$$

The T_1 time constant is influenced by the strength of the external magnetic field B_0, whereas the T_2 constant is not. However, the T_2 constant is heavily influenced by the homogeneity of the field, where more inhomogeneity leads to smaller T_2 constant values.

One of the major benefits of using NMR relaxometry is that it can tolerate inhomogeneity in the magnetic field [4, 8]. A process known as inversion recovery is used to obtain the T_1 parameter, and RF echoes are used to detect the T_2 value [8]. Specifically, a process of using spin-echo pulse sequences known as Carr-Purcell-Meiboom-Gill (CPMG) helps compensate for magnetic field inhomogeneity [19]. By measuring the T_1 and T_2 relaxation parameters, a sample can be identified similar to NMR spectroscopy. These techniques are not nearly as sensitive to magnetic field homogeneity as the chemical shift in NMR spectroscopy: in contrast to NMR spectroscopy which requires homogeneity on the order of 1-10 ppm, NMR relaxometry can tolerate homogeneities of 1000-5000ppm, roughly three orders of magnitude higher than spectroscopy [7, 19]. This makes relaxometry an incredibly appealing alternative for low-cost NMR solutions which lack the homogeneity required for NMR spectroscopy.

Chapter 3

Magnet Design in NMR Instrumentation

3.1 Superconducting Magnets

As NMR spectroscopy technology developed over the past decades, researchers wished to examine increasingly large chemical compounds. To examine these compounds, NMR spectrometers continued to increase magnetic field strength. Because chemical shift scales proportionally to magnetic field strength, larger fields would create larger chemical shift dispersion for easier analysis [4]. To achieve the higher magnetic field strength, most commercial NMR machines today use superconducting magnets to achieve magnetic field strength on the order of 5-20 T.

However, these machines have significant drawbacks. They are expensive to maintain as the superconducting magnets require cryogenic cooling to operate. These large magnets also consume a large amount of physical space such that entire laboratories are devoted to housing NMR spectrometers. These limitations prevent many researchers from having access to NMR instrumentation.

3.2 Low-Field Alternatives

Many researchers have realized the need for magnets that are smaller, cheaper, and portable in NMR applications. These smaller magnets generate weaker magnetic fields than the superconducting magnets, although recent improvements in permanent magnet technology (specifically rare earth magnets) have allowed for increasingly strong portable magnets [29]. In theory, decreasing the magnetic field strength will only lower the Larmor frequency of the sample. There is no minimum magnetic field strength for NMR to occur, as it has even been proven to work with the earth's magnetic field of roughly 25-65 μT [25].

However, problems with scaling down the magnetic field arise with homogeneity. It is increasingly difficult to maintain a homogeneous magnetic field at lower field strengths, which decreases the resolution of the sample signal as discussed in section 2.3.3. This problem is somewhat overcome by scaling down the size of the sample as well; if the sample is smaller, it interacts with a smaller section of the magnetic field which yields relatively higher magnetic field homogeneity.

There are multiple commercial desktop/benchtop NMR devices available today which use low-field permanent magnets [4, 19, 20, 24, 26, 27]. These devices typically use magnets from 0.1-2T, with the newer spectrometers using the higher field strengths. Some systems apply shimming coils and spinning to improve homogeneity, while others accept that resolution will be degraded. However, for some applications a tradeoff of frequency resolution compared

to cost and portability may favor these benchtop systems. Current research is being devoted to creating magnets that have high homogeneity and are inexpensive and light [3, 4, 7, 10, 11, 17, 19, 20, 24, 26, 27, 28, 29].

3.2.1 Halbach Array

In the early days of NMR spectroscopy, the magnetic fields were generated by permanent magnets. For example, the traditional "C-magnet" was used as it was the only magnet available [29]. In 1979, Klaus Halbach published work describing a circular array of magnets that would produce a uniform magnetic field [13, 14]. However, as superconducting magnets became available, NMR devices began to use these superior magnets as they provided stronger fields and thus better resolution. Now that there is a push to miniaturize magnets, the Halbach array has reappeared.

The Halbach array theory is shown in Figure 3.1 below. By arranging individual magnets in the following orientation, a uniform magnetic field is created in the center. Unlike other magnet designs, the magnetic field in a Halbach array is parallel to the face of the array and not perpendicular, which allows for easier RF coil and senor integration [3]. However, for a truly uniform center, a continuous magnetic ring with variable field direction would be necessary. With individual point magnets, the Halbach array cannot be completely uniform in the center. The more point magnets used, the closer performance gets to the ideal uniform center. Various implementations of the Halbach array are analyzed in Figure 3.2.

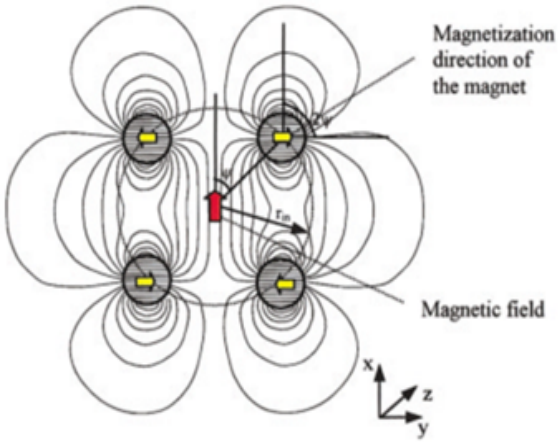

Figure 3.1: Magnetic field lines of theoretical Halbach array. Adapted from Moresi [20].

As Figure 3.2 displays, implementing an ideal Halbach array can be troublesome due to the distinct orientation and geometry of individual segments. In practice, the Halbach array is implemented with discrete point magnets, similar to items (g) and (h) in Figure 3.2. This magnetic configuration is known as a "mandhala", which is an acronym for 'Magnet Arrangements for Novel Discrete HAlbach LAyout' [24]. Recent research in miniaturizing NMR magnets focuses on the Halbach and mandhala designs due to its homogeneous design, achieving field strengths of up to 2T [11, 20, 24, 26, 27, 28].

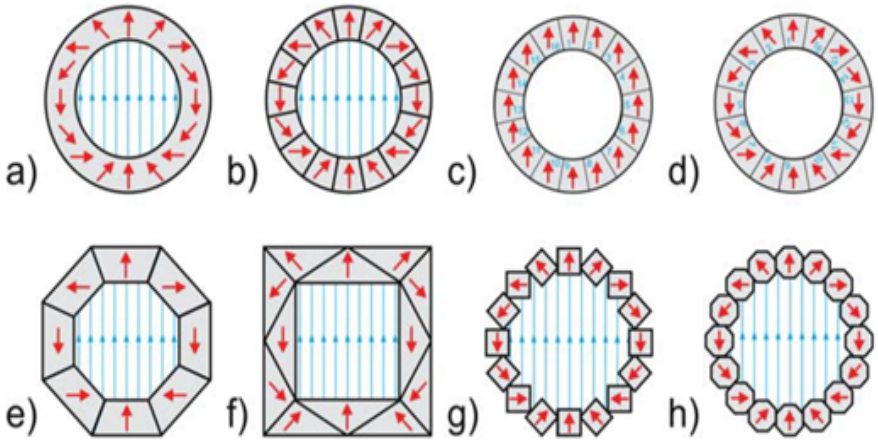

Figure 3.2: Different realizations of annular Halbach dipole: (a) ideal magnet; (b) discretized version of (a); (c) and (d) show how (b) could be made by cutting and rearranging pieces (indicated by a blue number) from a homogenously magnetized cylinder (c) by swapping segments symettric to the field axis (d); (e) octagonal magnet from trapezoidal pieces; (f) wedge design; (g) NMR-Mandhala (Magnet Arrangements for Novel Discrete Halbach Layout) with 16 elements of quadratic cross-section; (h) NMR-Mandhala with 16 elements of polygonal (octagonal) cross-section. (Flux lines are omitted in (c) and (d)). Adapted from Blümler [5].

Chapter 4

Experimental Setup

4.1 Point Magnets

In order to create a small, cost-effective magnet for NMR applications, a decision was made to use Neodymium permanent point-magnets. Each magnet is cylindrical with a height of 1/8" (3.175mm) and diameter of 3/16" (4.7625mm) as shown in Figure 4.1. Each neodymium dipole magnet, composed of a $Nd_2Fe_{14}B$ tetragonal crystalline structure and coated in nickel, has a magnetic field strength of approximately 0.3 T at its surface and has a N42 rating. The magnetic field has its poles at each of the circular surfaces of the cylinder. They are regarded as the strongest permanent magnet commercially available. Each magnet costs about $0.15, thus making it an incredibly cost-effective solution.

Point magnets were selected for this research because of their reconfigurability to create magnet designs of various shapes. For example, it is easy to configure the magnets into a Halbach array as well as experimenting with other magnet configurations. This flexibility allows for easily comparing different configurations in order to find the best design.

Figure 4.1: Neodymium point magnet used in magnet designs. Each magnet has a 5mm diameter and 3mm height with maximum field strength of 0.3 T at its surface.

4.2 Examined Magnet Configurations

Three distinct magnet configurations are examined in this report. Their designs are listed in the below subsections with results in Chapter 5.

4.2.1 Pentagonal/Hexagonal Plate

The first configuration analyzed was a simple pentagonal structure with a magnet in the center, seen in Figure 4.2(a). The thought behind this arrangement was that multiple magnets aligned in the same direction could increase the magnetic field observed. The magnets are placed on a metallic plate, so they do not require any adhesion. Each magnet is separated by their minimum distance (before the repulsive force overcame the attraction to the base metal plate), which was about 3mm. This was not inspired by any previous research but served more as a baseline for future measurements.

A modification of the pentagonal structure was made by adding a sev-

enth magnet, creating a hexagonal structure with a magnet in the middle, seen in Figure 4.2(b). This was done to increase the density of point magnets and hopefully increase field strength.

(a) (b)

Figure 4.2: Point magnet configurations for (a) Pentagonal arrangement with center magnet and (b) Hexagonal arrangement with center magnet.

4.2.2 Annulus

Our novel magnetic configuration design is an annulus with point magnets embedded inside. One half of the annulus has magnets with their north pole facing towards the center, while the other side has magnets with their south pole facing towards the center. The hope was that the symmetry of the magnets would create a unidirectional, uniform magnetic field in the center of the annulus as seen in Figure 4.3.

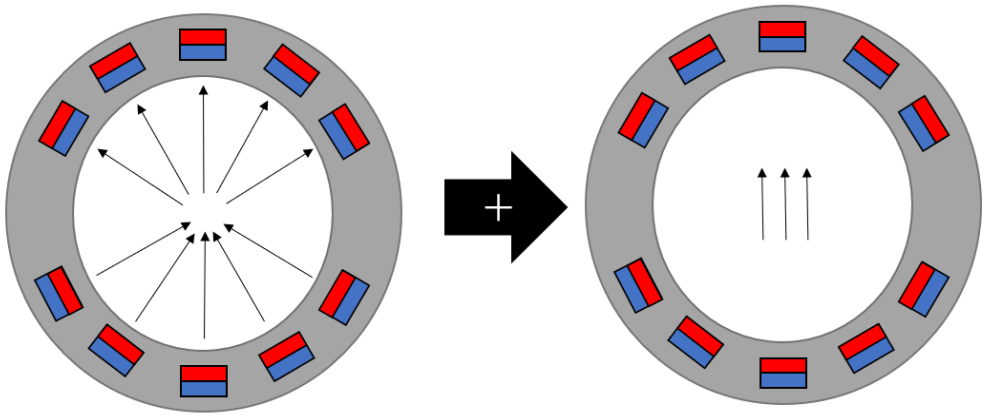

Figure 4.3: Theory behind annulus design (top-view). Each dipole point magnet produces a net magnetic field represented by an arrow, which if summed at the center should be uniformly pointing in a single direction.

A tradeoff in the annulus design is the radius versus number of magnets. If one desires to have a smaller radius to increase the field strength, the number of magnets that can fit in the annulus decreases. Four annuli were designed to examine this tradeoff, as seen in Figure 4.4. Data on this tradeoff is examined in Section 5.2.2.

All the annulus and Halbach array designs in Section 4.2.3 were created with a 3D printer using PLA plastic. CAD designs were created with "FreeCAD" software and printed on a CraftBot XL 3D printer. Magnets were then super-glued to the plastic. This enabled rapid prototyping and easy revisions while also being cost-effective.

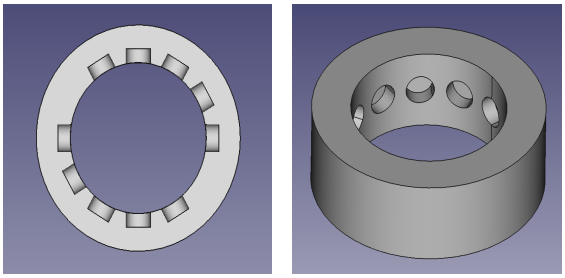

(a) 10 magnet annulus, 15mm radius

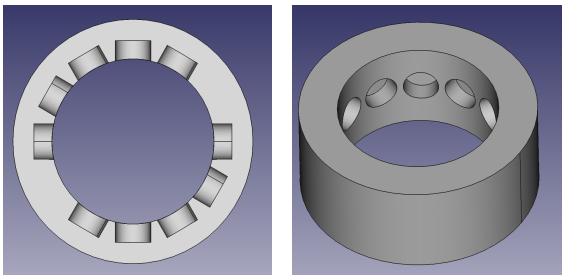

(b) 10 magnet annulus, 12.5mm radius

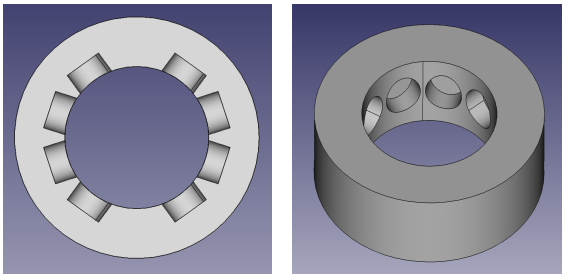

(c) 8 magnet annulus, 10mm radius

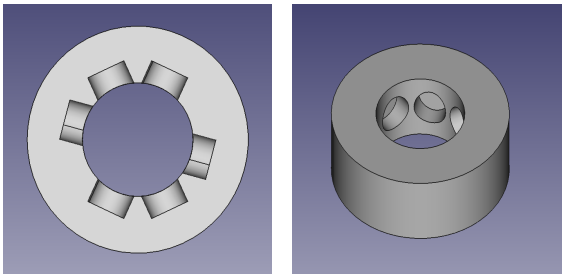

(d) 6 magnet annulus, 7.5mm radius

Figure 4.4: CAD schematics for various annulus designs. Four annuli were designed: (a) 15mm radius with 10 magnets, (b) 12.5mm radius with 10 magnets, (c) 10mm radius with 8 magnets, and (d) 7.5mm radius with 6 magnets.

4.2.3 Halbach Array

As mentioned in Section 3.2.1, a Halbach array is a magnet design that produces a unidirectional magnetic field. A Halbach array with 8 point magnets and radius of 10 mm was designed, as seen in Figure 4.5. After initial experiments, it was concluded an additional 16 magnet Halbach array with a 20mm radius should be constructed. Similar to the annuli, the Halbach arrays were 3D printed with magnets glued to the plastic.

4.3 Other Setup Details

To examine the strength of the magnetic field, the DC Gauss meter GM-1-ST from AlphaLab Inc. was used. Note that the gauss meter could only measure to 0.1 Gauss, and many measurements would have benefited from higher resolution. Standard laboratory stands and clamps were used to secure the magnets and gauss meter for measurement. The magnetic field was measured at various distances and positions for each magnet configuration, which is discussed in more detail in Chapter 5.

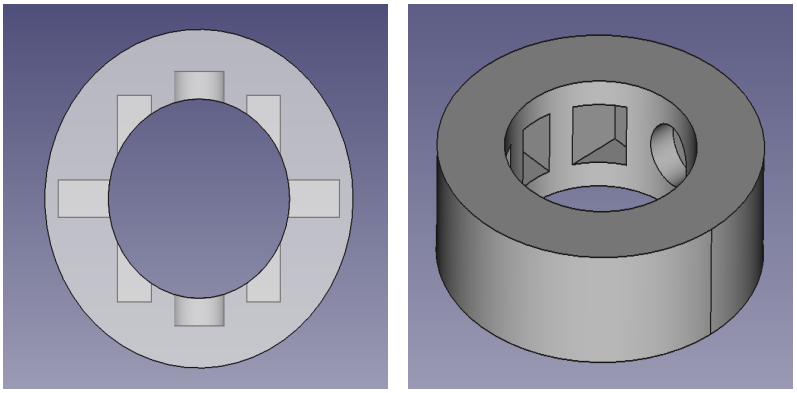

(a) 8 magnet annulus, 10mm radius

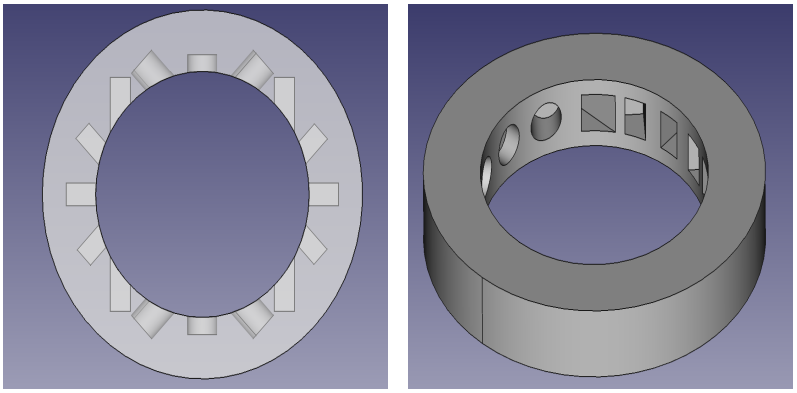

(b) 16 magnet annulus, 20mm radius

Figure 4.5: CAD schematics for Halbach Arrays. (a) 10mm radius with 8 magnets, (b) 20mm radius with 16 magnets.

Chapter 5

Results and Analysis

5.1 Simulated Results

Before obtaining measurements from the physical magnets, the magnetic field strength and uniformity were simulated for the multiple annuli and Halbach arrays. Simulations were done with QuickField FEA software and only supported two-dimensional simulations, which prevented simulating the pentagonal/hexagonal plate arrangements. Simulation results are found in Figure 5.1. The lighter colors represent stronger magnetic fields, which shows the Halbach arrays to be the most uniform of our designs.

5.2 Measured Results

5.2.1 Pentagon/Hexagon Plate: Baseline

The magnetic field strength was measured at varying distances for a single point magnet, the center magnet of the pentagonal configuration, and the center magnet of the hexagonal configuration as described in Section 4.2.1. These measurements served as a baseline for field strength in other configurations. As uniformity of field is not a concern for these configurations, it was not measured. Figure 5.2 shows the graphical results of field strengths.

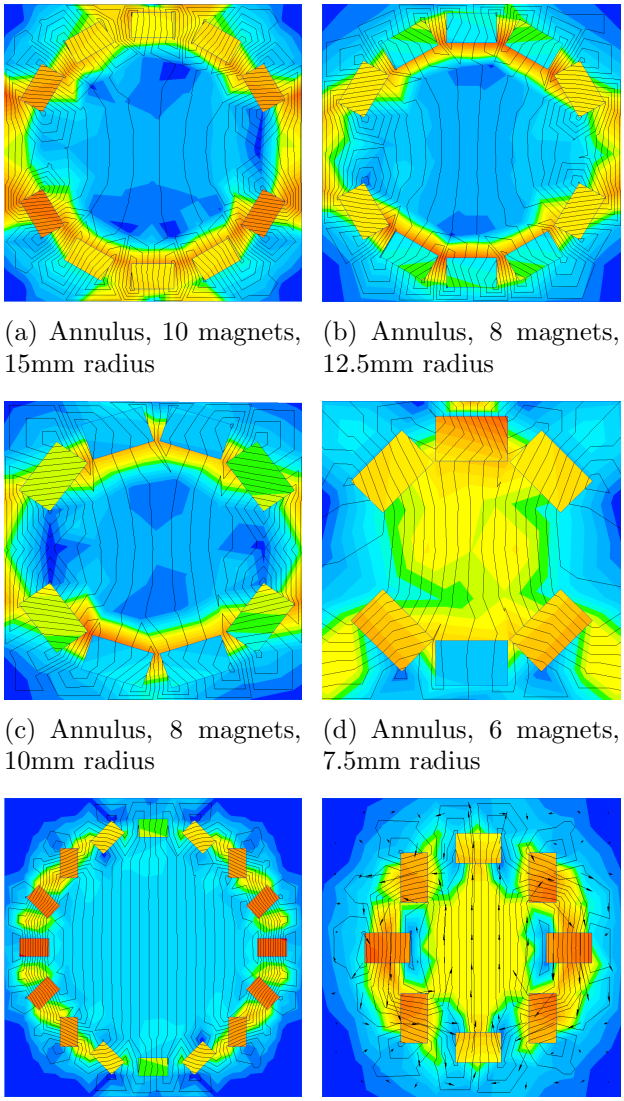

(a) Annulus, 10 magnets, 15mm radius

(b) Annulus, 8 magnets, 12.5mm radius

(c) Annulus, 8 magnets, 10mm radius

(d) Annulus, 6 magnets, 7.5mm radius

(e) Halbach Array, 16 magnets, 20mm radius

(f) Halbach Array, 8 magnets, 10mm radius

Figure 5.1: Magnetic Field strength simulations of various magnet configurations. Dark blue is the weakest and orange is the strongest. Both the annuli and Halbach arrays have magnetic fields pointing north in the center, but the Halbach arrays are both stronger and more uniform than their annulus counterparts.

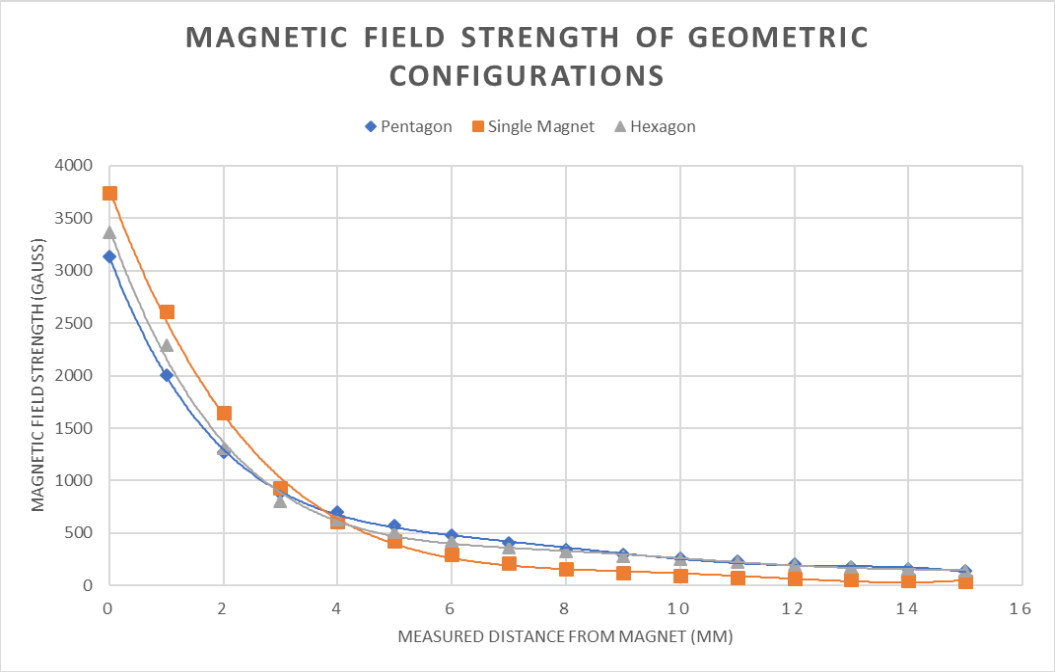

Figure 5.2: Graph of magnetic field strength versus distance for point magnet, pentagonal plate configuration, and hexagonal plate configuration.

At close distances, the single point magnet has the strongest magnetic field. This is most likely due to the lack of interference from other magnets, which is found in the pentagonal and hexagonal configurations. However, as the distance increases the pentagonal and hexagonal configurations become stronger than the single magnet due to the additive fields from multiple magnets. The pentagonal configuration is marginally stronger than the hexagonal configuration. These graphs also effectively demonstrate the $1/r^2$ degradation of field strength for a point magnet as distance increases.

5.2.2 Annuli and Halbach Array

Magnetic field data was recorded for each of the four annuli (15mm, 12.5mm, 10mm, and 7.5mm radii) as well as the 20mm and 10mm radius Halbach Arrays. Three trials were done for each magnet configuration and the average results are presented in Table 5.1.

Configuration	**Radius (mm)**	**Number Magnets**	**Magnetic Field (G)**	**Uniformity (ppm)**				
				10mm radius	***5mm radius***	***2mm radius***	***1mm radius***	***1mm X-axis***
Annulus	15	10	191.40	440439	121909	54859	22292	20550
Annulus	12.5	10	318.53	577752	151528	64671	19883	13709
Annulus	10	8	473.63	984306	272574	64677	27940	12809
Annulus	7.5	6	731.67	N/A	2512984	76492	25376	17039
Halbach Array	20	16	119.40	300949	65606	22055	5583	837
Halbach Array	10	8	479.60	1784959	307200	30164	8340	1251

Table 5.1: Magnetic Field strength and uniformity results for tested magnet configurations. The magnetic field strength is measured from the center of the magnet configuration, and uniformity measured over the given area.

The magnetic field strength reported for each configuration is the average field strength at the center of the magnet. Additionally, the uniformity is measured over a two-dimensional area instead of three-dimensions. This was done for simplicity, and the assumption is made that simply layering each magnet configuration will yield uniformity in three dimensions. The last column of Table 5.1 measures the uniformity in the X-axis, which is defined as the axis perpendicular to the magnetic field direction (East-West).

For more in-depth annulus data, see Appendix A. For more in-depth Halbach array data, see Appendix B. The appendices provide visual representations of field strength and uniformity measurements for each configuration.

5.2.2.1 Field Strength Results

Figure 5.3 shows the magnetic field strength of all six configurations based on the data from Table 5.1. The 7.5mm annulus has the highest magnetic field strength, which is not surprising due to the $1/R^2$ field strength decay. The 10mm annulus and Halbach array have comparable field strengths.

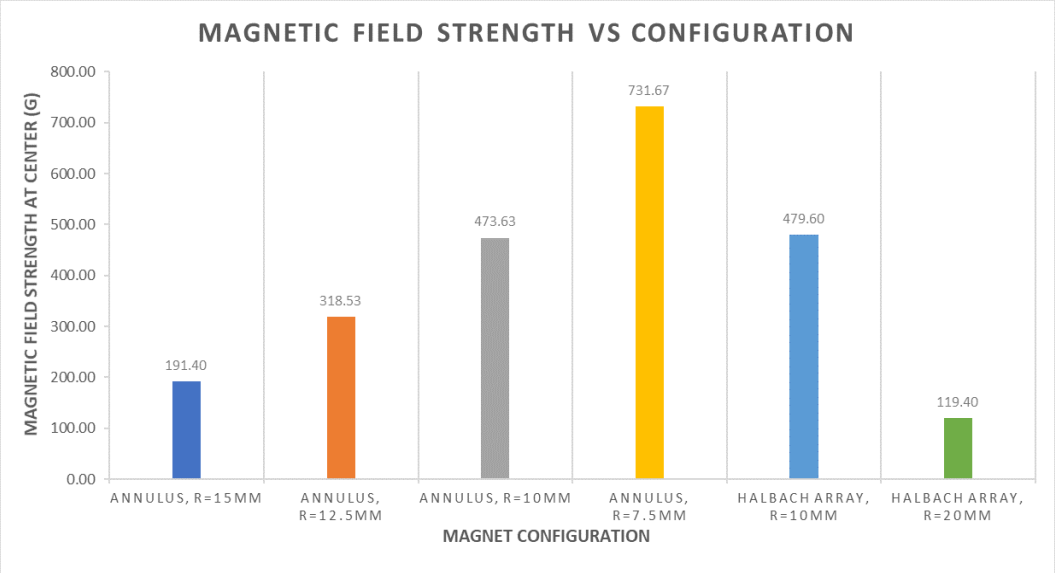

Figure 5.3: Graph of magnetic field strength versus configuration (Annuli and Halbach Arrays).

Table 5.2 compares the magnetic field strength of all configurations to the baseline measurements at the equivalent distance. It shows that all configurations improve over the baseline, but there is a tradeoff between the number of magnets and radius. If the radius is to decrease, the number of magnets must also decrease as it cannot fit into the configuration. It is also

interesting to note the last column of the table, which shows the ratio of magnetic field strength to the magnet rating of 0.3 T (3000 G).

Configuration	**Radius (mm)**	**Number Magnets**	**Magnetic Field (G)**	**Relative Increase (Single)**	**Relative Increase (Pentagon)**	**Relative Increase (Hexagon)**	**Percent Utilization**
Annulus	15	10	191.40	4.691	1.389	1.343	6.38%
Annulus	12.5	10	318.53	4.891	1.568	1.616	10.62%
Annulus	10	8	473.63	4.820	1.812	1.906	15.79%
Annulus	7.5	6	731.67	3.449	1.782	2.018	24.39%
Halbach Array	20	16	119.40	5.482	1.551	3.015	3.98%
Halbach Array	10	8	479.60	4.881	1.835	1.930	15.99%

Table 5.2: Magnetic field strength of configurations relative to baseline, as discussed in Section 5.2.1. All configurations improve over the baseline, with the 20mm Halbach Array having most overall improvement.

5.2.2.2 Uniformity Results

Figure 5.4 shows the uniformity measurements of all configurations based on the data in Table 5.1. Data was obtained by measuring the magnetic field strength over a given area and determining the maximum difference between all points within the area and the center. The X-axis shows the areas used to obtain uniformity measurements; the largest area measured a 10mm radius from the center of the configuration, while the smallest measured a 1mm distance on the X-axis (one-dimension). Uniformity is measured in parts-per-million (ppm).

Intuitively, the larger magnet configurations have greater uniformity (smaller ppm measurement) when measured over a large area. Also intuitively, uniformity improves as the measured area decreases. However, the important takeaways from Figure 5.4 are the relative uniformity measurements.

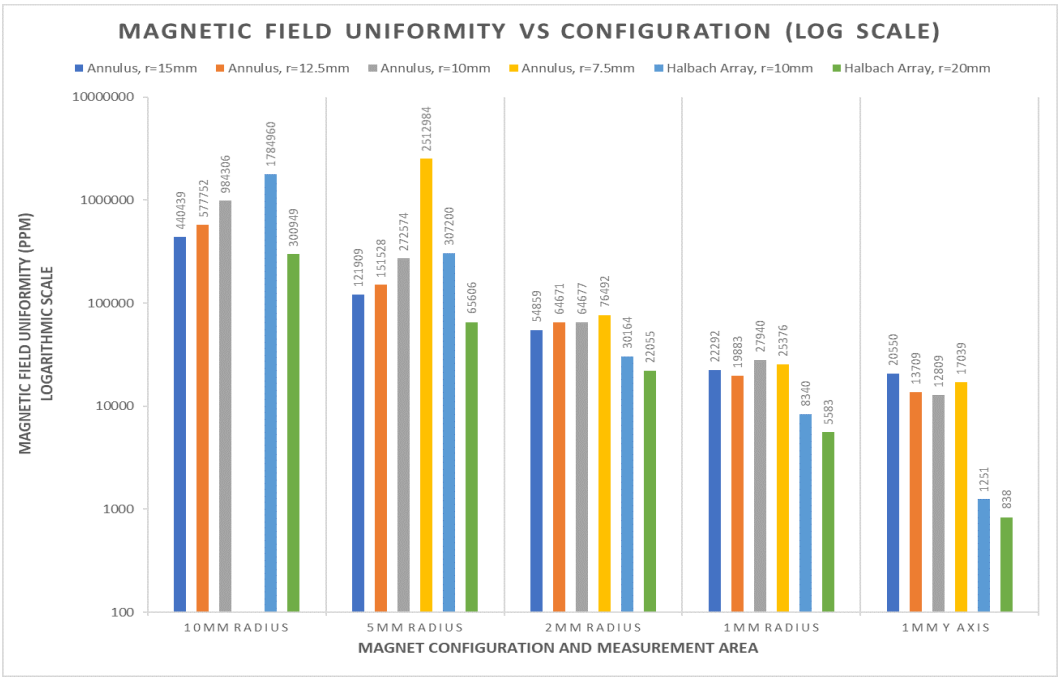

Figure 5.4: Graph of magnetic field uniformity versus configuration (Annuli and Halbach Arrays). Uniformity measured on a logarithmic scale.

For example, the 7.5mm annulus consistently has the worst uniformity compared to other magnet configurations. Additionally, the Halbach arrays have the best uniformity. The 20mm Halbach array consistently has the best uniformity, while the 10mm Halbach array has better uniformity than the annuli only at sufficiently small measurement areas. However, Halbach array uniformity only improves dramatically from other configurations at the 1mm X-axis measurement. Also interesting to note is that the Halbach array performs much better in the X-axis (perpendicular to magnetic field) than in the Y-axis (parallel to the magnetic field).

Chapter 6

Analysis and Future Work

This chapter will build off the data in Chapter 5 and analyze the results. Also presented are ideas for future work in this area of research.

6.1 Analysis

It is crucial to remember that as discussed in Sections 2.3.3 and 2.4, the most important aspect of an NMR magnet is its homogeneity/uniformity. An NMR signal can be obtained at any field strength, but only when the magnet is sufficiently uniform can it be used for detecting chemical shifts and relaxometry. Therefore, the majority of analysis is based on homogeneity.

The only notable result regarding field strength is that the 10mm Halbach Array shows no improvement of field strength over the 10mm annulus. This indicates the point magnet distance and decay of $1/r^2$ is much more significant in determining field strength than the configuration itself. Rather, the configuration is meant to provide significant benefits in uniformity.

When analyzing the magnet uniformity, it is important to realize the uniformity is only needed over the given sample volume. For example, if measuring a sample with a 2.5mm radial cross-area, the 10mm radius uniformity

measurement is inappropriate. Rather, the 5mm and 2mm radius uniformity measurements should be considered, as they better match the sample area. For standard NMR measurements, a sample tube has a 5mm outer diameter and 4.2mm inner diameter. However, smaller sample tubes with 3mm outer diameter and 2.4mm inner diameter are also used [7]. Therefore, the 2mm and 1mm radius uniformity measurements are most applicable for analysis. As seen in Table 5.1 and Figure 5.4, the Halbach arrays have the greatest uniformity for the 2mm and 1mm radial uniformity measurements.

Table 6.1 shows the Halbach array uniformity measurements compared to the minimum values required for different NMR technologies. It is clear that the Halbach arrays do not have the required uniformity to perform chemical shift analysis in NMR spectroscopy. However, the uniformity appears to be sufficient over small enough sample volumes to perform NMR relaxometry analysis. The Halbach arrays also could be used to simply measure large nuclei in a NMR spectroscopy setting, where the chemical shift is not necessary to measure. Additionally, the gauss meter could only record to 0.1 G, and higher resolution may have been able to measure smaller homogeneity changes, which would have improved our results.

Although the annuli were roughly comparable to the Halbach arrays in magnetic field strength, their uniformity is clearly insufficient for NMR applications. Barring any tremendous uniformity improvements, the annulus design should not be considered in this context. It was worth investigating these novel designs, however, the 20mm Halbach array is proven to be the

Halbach Radius	Measurement Area	Uniformity (ppm)	Chemical Shift (ppm)	Relaxometry (ppm)
10mm	2mm radius	30164	1-10 (small molecules)	1000-5000
	1mm radius	8430		
	1mm x-axis	1251		
20mm	2mm radius	22055	10-100 (large molecules)	
	1mm radius	5583		
	1mm x-axis	837		

Table 6.1: Halbach Array uniformity analysis. The 2mm and 1mm radial measurements indicate the Halbach arrays do not have necessary uniformity for chemical shifts, but could be used for NMR relaxometry over small enough sample volumes.

most effective magnet configuration for NMR miniaturization.

Given that the Halbach arrays were constructed with less than 20 magnets and cost under three dollars, the conclusion that it is an appropriate magnet for NMR relaxometry is very promising. Section 6.2 investigates ways to improve the uniformity even further and the next steps towards miniaturizing NMR.

6.2 Future Work

There are many possible methods for improving magnetic field homogeneity that were not investigated in this work. The most obvious method would be to attempt to add more magnets. Previous research has shown that a Halbach array can be created from nested arrays which improves both homogeneity and magnetic field strength [27]. Also fairly obvious, we could upgrade to stronger commercially available neodymium point magnets. Shim coils can

be used to improve homogeneity by up to two orders of magnitude by correcting magnetic field abnormalities [1]. It has been demonstrated that using iron disks to shield the NMR sample improves field homogeneity, which could be easily adapted to the presented design [7]. As shown in Section 2.3.3, spinning the sample averages out uniformity and improves the NMR signal resolution. Finally, by simply using a smaller sample the observed magnetic field is more uniform, thus improving the NMR signal [17]. These techniques could improve homogeneity in the presented design significantly and thus make the Halbach array presented more readily adoptable. Improvements in homogeneity could also make the Halbach array presented a viable solution for NMR spectroscopy, where the chemical shift could be adequately measured.

Although the presented Halbach array design is thought to support NMR relaxometry, future work should investigate whether this is true in practice. Using the presented Halbach array in a NMR spectrometer or relaxometer and measuring experimental signals would provide insight as to how well the magnet performs in reality. This research must be completed before considering building an entire miniaturized NMR device, which is the eventual goal of this work. Future work may investigate building custom RF probes and hardware to measure NMR signals from the Halbach array and comparing measurements to commercially available devices.

The analysis to this point has been based on the assumption that homogeneity is critical for NMR measurements. However, with new advancements in data analysis via machine learning algorithms, perhaps this assumption no

longer holds. When the NMR signal is analyzed in a non-uniform magnetic field, perhaps new features could be extracted from that data that were previously regarded as noise. A non-uniform magnetic field may actually provide more information about a sample than current analyses. Future research aims to use machine learning algorithms to investigate NMR signals for new information and determine if non-uniformity can provide more data than previously thought.

Chapter 7

Conclusions

This report has shown that cheap, portable point magnets can be used to create a suitable magnet for NMR applications. Although the annulus designs proved insufficient, by utilizing the Halbach array design and a 3-D printer, multiple magnet configurations can be made with appropriate magnetic field homogeneity needed for NMR relaxometry. With some inexpensive modifications, the Halbach arrays may even have sufficient homogeneity for NMR spectroscopy and measuring chemical shifts. The presented magnets may also be useful in a new application of NMR where machine learning is used to extract previously hidden data from noisy signals. Future research is required to use the magnets to obtain real NMR measurements and determine signal resolution and capabilities, but initial results look promising. With these advancements in NMR magnets, miniaturized NMR devices can be produced to explore new domains. Within a few years, it is possible hand-held devices using magnets similar to the ones presented could use NMR for quick chemistry measurements, medical diagnostics, and beyond.

Appendices

Appendix A

Annulus Measurement Data

This appendix provides more complete measurement data for the annuli. Specifically, Figures A.1-A.4 display magnetic field strength and uniformity measurements in a graphical representation. These values were obtained after three trials of measurements at different locations within the annuli.

Each cell with a M is a representation of a point magnet's location. The N and S cells indicate the overall magnetic field direction. The other cells contain measurement information in that relative location within the annulus.

The left column measurements are 5mm apart, while the right column are 1mm apart. The top row indicates the magnetic field strength in Gauss at the particular location, with green indicating higher strength. The bottom row indicates the percent difference of each location compared to the center, with green indicating smaller difference.

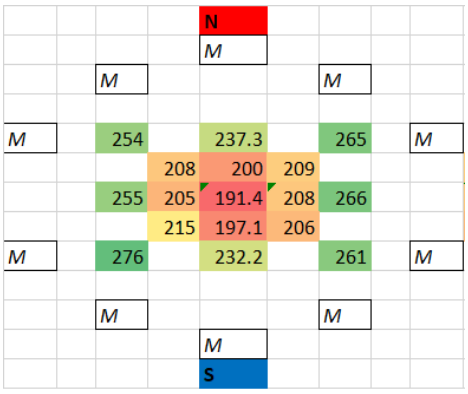

(a) Field strength, measurements 5mm apart.

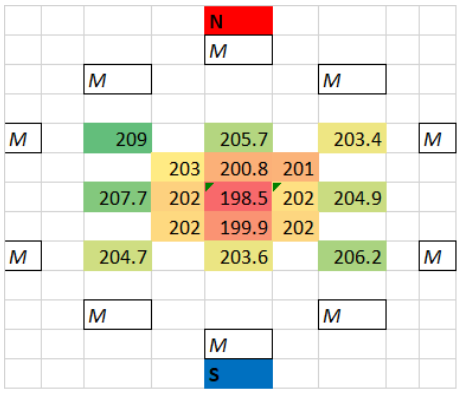

(b) Field strength, measurements 1mm apart.

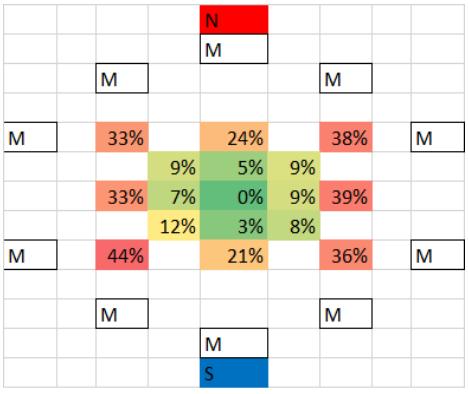

(c) Percent difference from center of magnet, measurements 5mm apart.

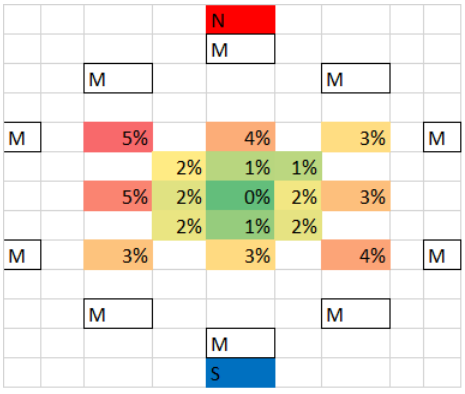

(d) Percent difference from center of magnet, measurements 1mm apart.

Figure A.1: Magnetic field strength and uniformity measurements for 15mm radius annulus, using 10 magnets.

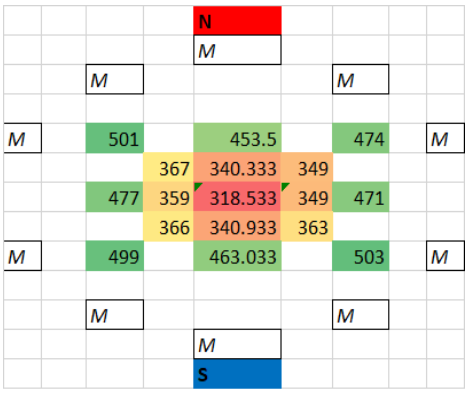

(a) Field strength, measurements 5mm apart.

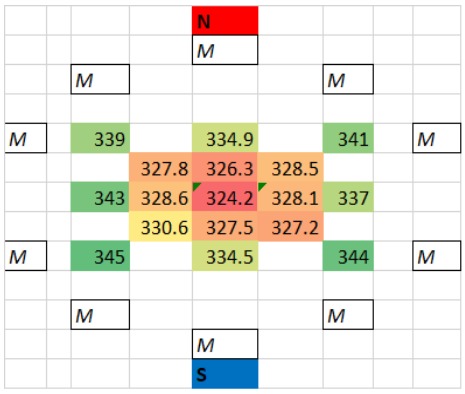

(b) Field strength, measurements 1mm apart.

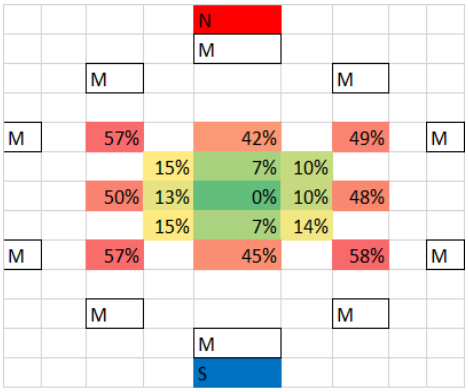

(c) Percent difference from center of magnet, measurements 5mm apart.

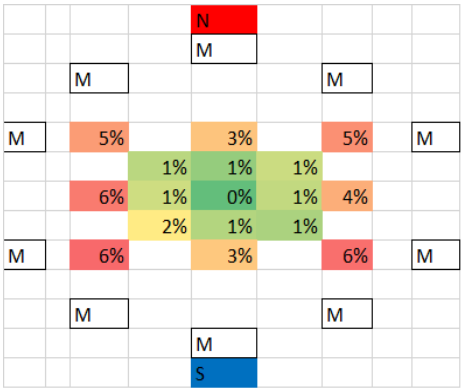

(d) Percent difference from center of magnet, measurements 1mm apart.

Figure A.2: Magnetic field strength and uniformity measurements for 12.5mm radius annulus, using 10 magnets.

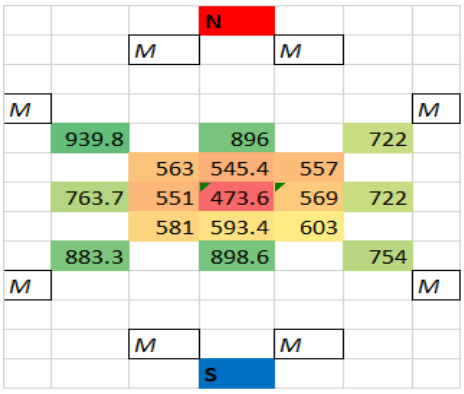

(a) Field strength, measurements 5mm apart.

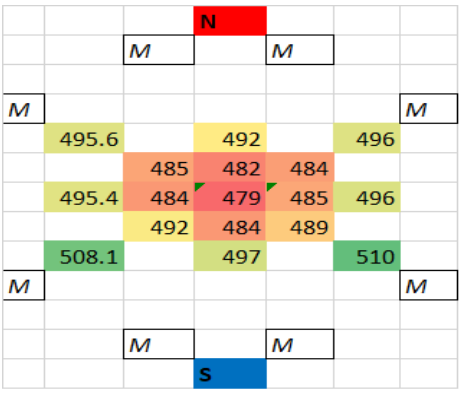

(b) Field strength, measurements 1mm apart.

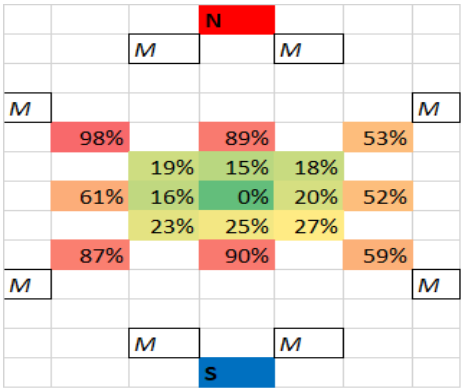

(c) Percent difference from center of magnet, measurements 5mm apart.

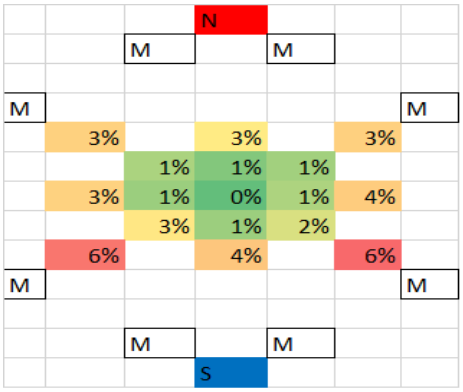

(d) Percent difference from center of magnet, measurements 1mm apart.

Figure A.3: Magnetic field strength and uniformity measurements for 10mm radius annulus, using 8 magnets.

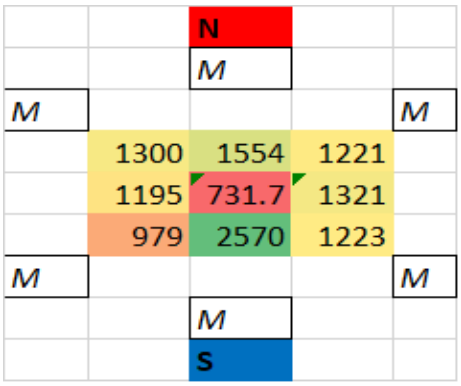

(a) Field strength, measurements 5mm apart.

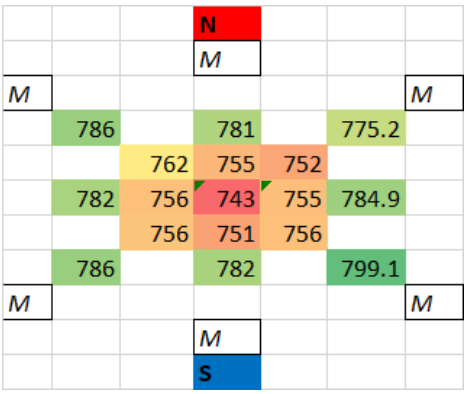

(b) Field strength, measurements 1mm apart.

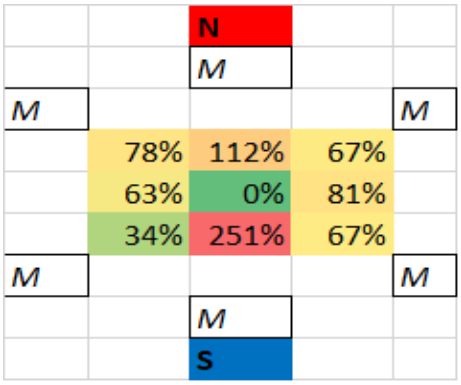

(c) Percent difference from center of magnet, measurements 5mm apart.

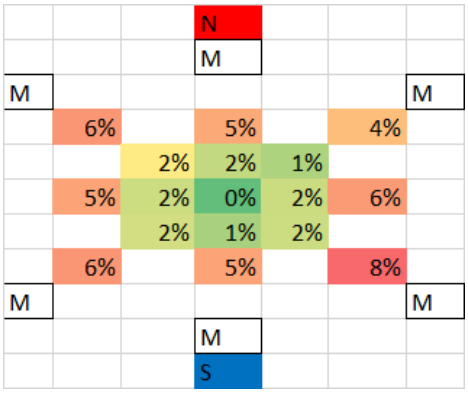

(d) Percent difference from center of magnet, measurements 1mm apart.

Figure A.4: Magnetic field strength and uniformity measurements for 7.5mm radius annulus, using 6 magnets.

Appendix B

Halbach Array Measurements

Similar to Appendix A, this appendix provides more complete measurement data for the Halbach Array. Figure B.1 displays magnetic field strength and uniformity measurements in a graphical representation. These values were obtained after three trials of measurements at different locations within the Halbach array.

Each cell with a M is a representation of a point magnet's location. The N and S cells indicate the overall magnetic field direction. The other cells contain measurement information in that relative location within the Halbach array.

The left column measurements are 5mm apart, while the right column are 1mm apart. The top row indicates the magnetic field strength in Gauss at the particular location, with green indicating higher strength. The bottom row indicates the percent difference of each location compared to the center, with green indicating smaller difference.

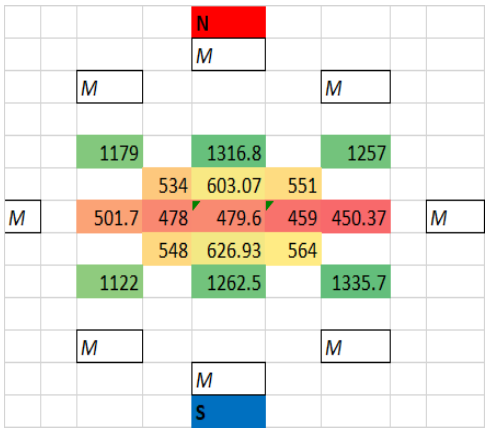

(a) Field strength, measurements 5mm apart.

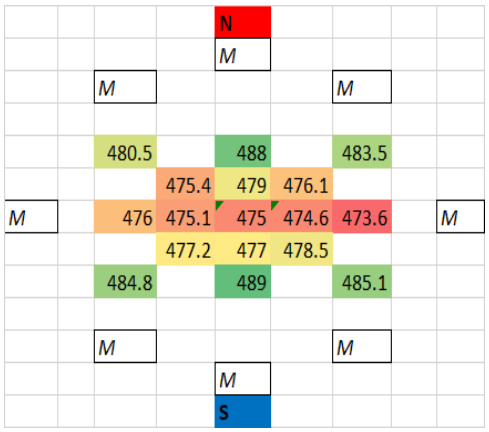

(b) Field strength, measurements 1mm apart.

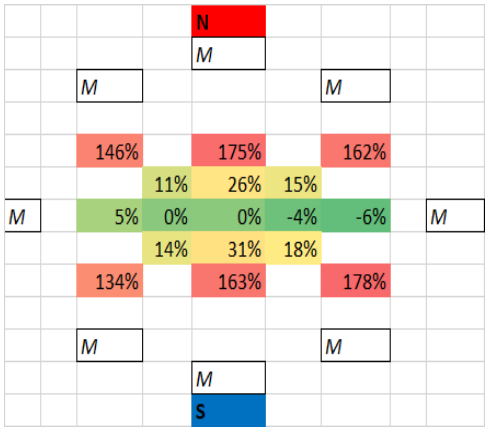

(c) Percent difference from center of magnet, measurements 5mm apart.

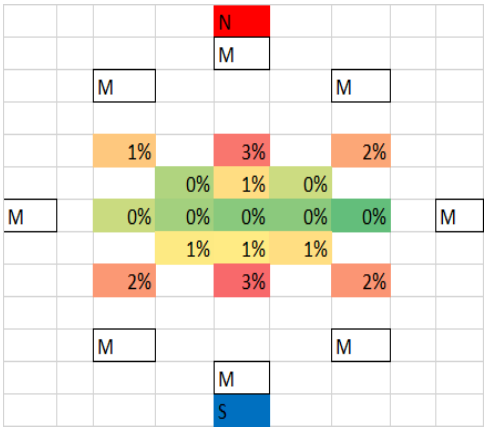

(d) Percent difference from center of magnet, measurements 1mm apart.

Figure B.1: Magnetic Field strength and uniformity measurements for the 10mm radius Halbach Array, using 8 magnets.

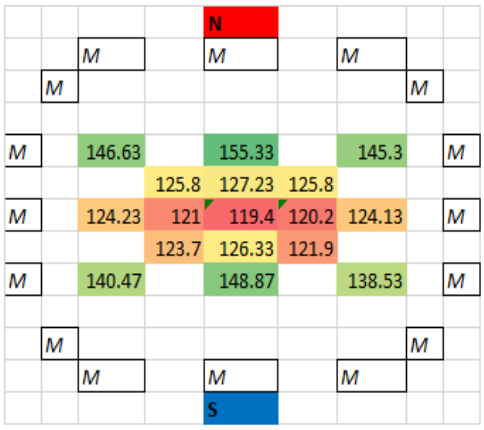

(a) Field strength, measurements 5mm apart.

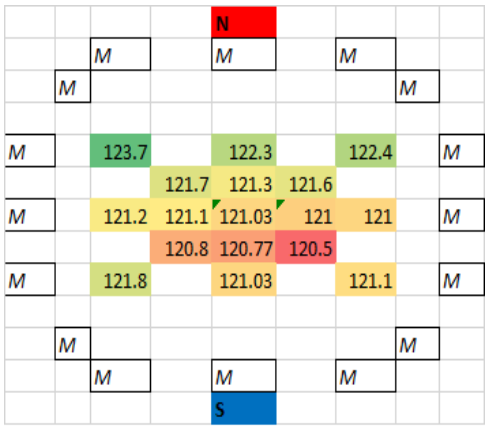

(b) Field strength, measurements 1mm apart.

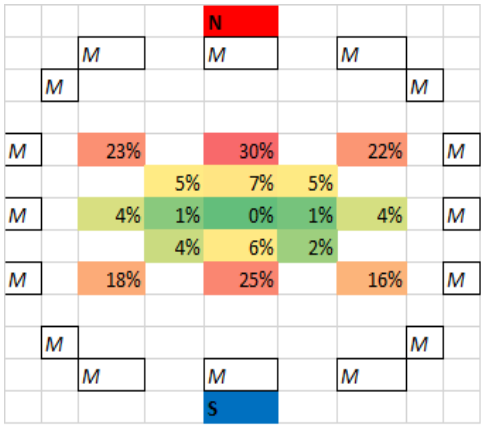

(c) Percent difference from center of magnet, measurements 5mm apart.

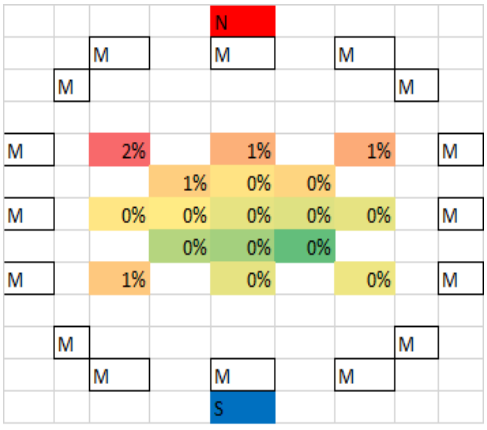

(d) Percent difference from center of magnet, measurements 1mm apart.

Figure B.2: Magnetic Field strength and uniformity measurements for the 20mm radius Halbach Array, using 16 magnets.

Bibliography

[1] Weston A. Anderson. Electrical current shims for correcting magnetic fields. *Review of Scientific Instruments*, 32(3):241–250, 1961.

[2] Edwin D. Becker. *High Resolution NMR: Theory and Chemical Applications*. Academic Press, San Diego, 3rd edition, 2000.

[3] B. Blümich, J. Perlo, and F. Casanova. Mobile single-sided nmr. *Progress in Nuclear Magnetic Resonance Spectroscopy*, 52(4):197–269, 2008.

[4] Bernhard Blümich, Federico Casanova, and Stephan Appelt. Nmr at low magnetic fields. *Chemical Physics Letters*, 477(4-6):231–240, 2009.

[5] Peter Blümler and Federico Casanova. *CHAPTER 5. Hardware Developments: Halbach Magnet Arrays*, pages 133–157. New Developments in NMR. Royal Society of Chemistry, 2016.

[6] F. Bloch. Nuclear induction. *Physical Review*, 70(7-8):460–474, 1946.

[7] K. Chonlathep, T. Sakamoto, K. Sugahara, and Y. Kondo. A simple and low-cost permanent magnet system for nmr. *Journal of Magnetic Resonance*, 275:114–119, 2017.

[8] David P. Cistola and Michelle D. Robinson. Compact nmr relaxometry of human blood and blood components. *Trends in analytical chemistry :*

TRAC, 83(A):53–64, 2016.

[9] F. Dalitz, M. Cudaj, M. Maiwald, and G. Guthausen. Process and reaction monitoring by low-field nmr spectroscopy. *Progress in Nuclear Magnetic Resonance Spectroscopy*, 60:52–70, 2012.

[10] E. Danieli, J. Mauler, J. Perlo, B. Blumich, and F. Casanova. Mobile sensor for high resolution nmr spectroscopy and imaging. *Journal of Magnetic Resonance*, 198(1):80–7, 2009.

[11] E. Danieli, J. Perlo, B. Blumich, and F. Casanova. Small magnets for portable nmr spectrometers. *Angew Chem Int Ed Engl*, 49(24):4133–4135, 2010.

[12] Walther Gerlach and Otto Stern. Der experimentelle nachweis der richtungsquantelung im magnetfeld. *Zeitschrift für Physik*, 9(1):349–352, 1922.

[13] K. Halbach. Strong rare earth cobalt quadrupoles. *IEEE Transactions on Nuclear Science*, 26(3):3882–3884, 1979.

[14] K. Halbach. Design of permanent multipole magnets with oriented rare earth cobalt material. *Nuclear Instruments and Methods*, 169, 1980.

[15] B. P. Hills, K. M. Wright, and D. G. Gillies. A low-field, low-cost halbach magnet array for open-access nmr. *Journal of Magnetic Resonance*, 175(2):336–9, 2005.

[16] Joseph P. Hornak. The basics of nmr. `https://www.cis.rit.edu/htbooks/nmr/inside.htm`. Accessed: 2018-09-11.

[17] D. Issadore, C. Min, M. Liong, J. Chung, R. Weissleder, and H. Lee. Miniature magnetic resonance system for point-of-care diagnostics. *Lab Chip*, 11(13):2282–7, 2011.

[18] P. C. Lauterbur. Image formation by induced local interactions: Examples employing nuclear magnetic resonance. *Nature*, 242:190, 1973.

[19] Hakho Lee, Eric Sun, Donhee Ham, and Ralph Weissleder. Chip–nmr biosensor for detection and molecular analysis of cells. *Nature Medicine*, 14:869, 2008.

[20] Giorgio Moresi and Richard Magin. Miniature permanent magnet for table-top nmr. *Concepts in Magnetic Resonance*, 19B(1):35–43, 2003.

[21] W. G. Proctor and F. C. Yu. The dependence of a nuclear magnetic resonance frequency upon chemical compound. *Physical Review*, 77(5):717–717, 1950.

[22] E. M. Purcell, H. C. Torrey, and R. V. Pound. Resonance absorption by nuclear magnetic moments in a solid. *Physical Review*, 69(1-2):37–38, 1946.

[23] I. I. Rabi, J. R. Zacharias, S. Millman, and P. Kusch. A new method of measuring nuclear magnetic moment. *Physical Review*, 53(4):318–318, 1938.

[24] H. Raich and P. Blümler. Design and construction of a dipolar halbach array with a homogeneous field from identical bar magnets: Nmr mandhalas. *Concepts in Magnetic Resonance Part B: Magnetic Resonance Engineering*, 23B(1):16–25, 2004.

[25] J. Stepišnik, V. Eržen, and M. Kos. Nmr imaging in the earth's magnetic field. *Magnetic Resonance in Medicine*, 15(3):386–391, 1990.

[26] M. C. D. Tayler and D. Sakellariou. Low-cost, pseudo-halbach dipole magnets for nmr. *Journal of Magnetic Resonance*, 277:143–148, 2017.

[27] Paulo V. Trevizoli, Jaime A. Lozano, Guilherme F. Peixer, and Jader R. Barbosa Jr. Design of nested halbach cylinder arrays for magnetic refrigeration applications. *Journal of Magnetism and Magnetic Materials*, 395:109–122, 2015.

[28] P. Wróblewski, J. Szyszko, and W. T. Smolik. Mandhala magnet for ultra low-field mri. In *2011 IEEE International Conference on Imaging Systems and Techniques*, pages 248–252, 2011.

[29] Sergey S. Zalesskiy, Ernesto Danieli, Bernhard Blümich, and Valentine P. Ananikov. Miniaturization of nmr systems: Desktop spectrometers, microcoil spectroscopy, and "nmr on a chip" for chemistry, biochemistry, and industry. *Chemical Reviews*, 114(11):5641–5694, 2014.

Vita

John Grant MacKay was born in Hartford, Connecticut on August 22, 1995, the son of Michael F. MacKay and Jane P. MacKay. He grew up in Baltimore, Maryland and then moved to St. Louis, Missouri in 2013 to attend undergrad. He received two Bachelor of Science degrees from Washington University in St. Louis in 2017: one in Computer Engineering and the other in Electrical Engineering. He then started graduate school at The University of Texas at Austin in August 2017 for Electrical and Computer Engineering, specializing in the Architecture, Computer Systems, and Embedded Systems (ACSES) track. He will graduate with a Master of Science in Engineering in May 2019. Following graduation, he will begin his career at Apple Inc. as a Design Verification Engineer in the Media and Neural Engines group in Austin, Texas.

Permanent Email Address: jgmackay@utexas.edu

This report was typeset with LaTeX[†] by the author.

[†]LaTeX is a document preparation system developed by Leslie Lamport as a special version of Donald Knuth's TeX Program.